DYNAMICAL CHARACTERISTICS AND ANALYSIS OF A PUPILLARY LIGHT REFLEX MODEL

A Project Report

submitted by

AMIT M. WARRIER

(EE09B004)

in partial fulfilment of the requirements
for the award of the degree of

BACHELOR OF TECHNOLOGY
in
ELECTRICAL ENGINEERING

DEPARTMENT OF ELECTRICAL ENGINEERING
INDIAN INSTITUTE OF TECHNOLOGY, MADRAS.

May 14, 2013

PROJECT CERTIFICATE

This is to certify that the project titled **DYNAMICAL CHARACTERISTICS AND ANALYSIS OF A PUPILLARY LIGHT REFLEX MODEL**, submitted by **Amit M. Warrier (EE09B004)**, to the Indian Institute of Technology, Madras, for the award of the degree of **Bachelor of Technology**, is a bona fide record of the project work done by him under my supervision. The contents of this report, in full or in parts, have not been submitted to any other Institute or University for the award of any degree or diploma.

Prof. G. Raina
Project Guide
Professor
Dept. of Electrical Engineering
IIT Madras, Chennai 600 036

Prof. S. E. Bhattacharya
Head
Dept. of Electrical Engineering
IIT Madras, Chennai 600 036

Place: Chennai

Date: May 22, 2013

ACKNOWLEDGEMENTS

I would first like to thank Dr. Gaurav Raina for his guidance throughout the course of this project. He has taught me the importance of framing a scientific argument along with presenting sound analysis.

Special thanks to Anand Krishnamurti Rao, my batchmate, with whom I have worked with for a year in completing this project.

I also thank Nizar Malangadan and Haseen Rahman for help figuring out the various software used to conduct the analysis in this project.

ABSTRACT

KEYWORDS: physiological models; local stability; rate of convergence; Hopf bifurcation; robustness.

Mathematical models for pupillary light reflex are well documented in the literature. But research has focused primarily on the biological aspects of the pupillary response. Analysis from the perspective of design requires techniques from control theory and dynamical systems analysis.

In this paper, we investigate a non-linear, time delayed model of pupillary light reflex. Using time and frequency domain analysis, we study its stability properties and offer guidelines on parameter values, that guarantee local stability. Trade-offs between system parameters are explored with the help of stability charts. It is shown that a desired rate of convergence can be achieved in the transient response by tuning parameters appropriately. The robustness of the model is measured for uncertainties in parameter values using the Vinnicombe metric. We prove that each parameter can induce a loss in stability via a Hopf bifurcation. Further, the stability and periodicity of the ensuing limit cycles are characterised analytically using normal forms and centre manifold theorem. Bifurcation diagrams accompany our results. We establish that the limit cycles generated are always stable in nature. In fact, large neural constants give rise to limit cycles through a subcritical Hopf, which is undesirable. The analysis reveals that the pupillary reflex model is not easy to control once it loses stability. Our work provides design-friendly guidelines to ensure stability and achieve a desired level of performance and robustness.

TABLE OF CONTENTS

LIST OF FIGURES

NOTATION

A^*	Steady-state area of pupil, mm^2
I^*	Equilibrium intensity of incoming light, $lumens/mm^2$
α	Rate constant for pupillary movements
γ	Rate constant for the neural firing frequency
α	Pupillary latency

CHAPTER 1

Introduction

Biological systems as they exist today are the result of years of evolution. Analysing biological phenomena as dynamical systems involves a reverse engineering process. A model is first proposed, and then continually fine-tuned to resemble the actual response as closely as possible. A thorough investigation of the model in terms of stability, transient behaviour and robustness is a critical requirement for system designers. One aspect of biological systems that makes this analysis challenging is the time delayed response of the feedback. Our paper focuses on a model of pupillary light reflex, the mechanism that adjusts the area of the pupil according to the intensity of light falling on it.

The phenomenon of pupillary light reflex was first studied as a mathematical model in (9). This paved the way for further analysis in the field. The authors of (6) investigated the mechanism from a control theoretic perspective. Their equation is used as the basis for any advanced research in the subject today. Some of the biological aspects of the mechanism were analysed in (3) (4), in an attempt to understand the cause of the time delay. The focus of research has been to fine-tune existing models to better characterize pupillary reflex, and relate it to other physiological responses. However, our work investigates the problem from a design point of view, through key performance metrics like stability, rate of convergence and robustness.

The focus of our analysis is the non-linear, time delayed model of pupillary light reflex proposed in (6). We derive a linear transfer function model, showing that the delay is an intrinsic parameter and not in the feedback. In terms of analysis, we perform both a local stability and a local bifurcation analysis. We establish the necessary and sufficient condition for local stability. A sufficient condition for stability independent of the time delay is also proposed. The rate of convergence in the stable region is analysed as a function of system parameters. The robustness of the model is determined for uncertainties in parameter

values using the Vinnicombe metric. We also explicitly show that variation in each parameter value can induce a loss of stability via a Hopf bifurcation. In each case, the stability of the ensuing limit cycles is analytically characterised using normal forms and the centre manifold theorem. Our analytical work is accompanied by stability charts and bifurcation diagrams.

Each of the results we derive with respect to the performance metrics are evaluated from the perspective of design. The sufficient conditions for stability offer less leeway in terms of parameter values, but are easier to satisfy. Trade-offs exist between the values of the neural delay, pupillary constant and neural constant in order to maintain stability. The transient behaviour of the pupillary response can be chosen to be underdamped or overdamped, as a function of parameter values. Allowable uncertainties in parameter values are measured so as to ensure robustness. We show that the limit cycles that arise via Hopf bifurcations are always stable. But they may go through a subcritical Hopf bifurcation in which case pupillary reflex becomes difficult to control once it slips into instability.

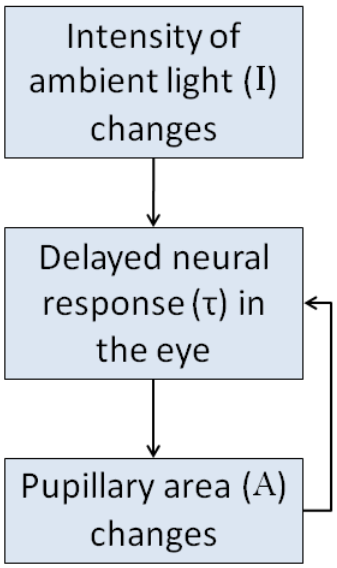

Figure 1.1: Phenomenon of pupillary light reflex according to the Longtin-Milton model. Change in the input intensity of light causes a change in pupil area. The delay is intrinsic to the response.

The rest of the paper is organised as follows. In Chapter 2, we introduce the Longtin-Milton model of pupillary reflex and linearise the associated delay-

differential equation. In Chapter 3, we construct conditions on the parameters that ensure local stability. The implications of these conditions are examined using stability charts. In Chapter 4, we analyse local rate of convergence as a function of parameter values. In Chapter 5, the robustness of the model is analysed for parameter uncertainties and in Chapter 6, a detailed Hopf bifurcation analysis is carried out. In Chapter 7, we summarise our results and mention avenues for further research.

CHAPTER 2

Model

In this chapter, we introduce the Longtin-Milton model (6) of pupillary light reflex. The associated delay-differential equation is linearised to carry out further analysis.

The authors of (6) used neurophysiological data to develop a model of pupillary light reflex. This is expressed in terms of the following non-linear delay differential equation

$$\frac{dg}{dA}\frac{dA(t)}{dt} + \alpha g(A) = \gamma \ln \frac{I(t-\tau)A(t-\tau)}{\hat{I}\hat{A}}, \tag{2.1}$$

where

$A(t) =$ area of the pupil at a time t,

$I(t) =$ intensity of light falling on the retina at a time t,

$\hat{I}, \hat{A} =$ threshold values of I, A below which there is no pupillary response,

$\tau =$ pupillary latency or *neural delay*,

$\alpha =$ rate constant for pupillary movements or *pupillary constant*,

$\gamma =$ rate constant for the neural firing frequency or *neural constant*, and

$g(A) =$ feedback function relating changes in iris muscle activity to changes in pupil area. The product $\phi(t) = I(t)A(t)$ is the retinal flux at time t.

Modelling the dynamics of pupillary response naturally involves certain biological constraints. The Longtin-Milton model accounts for the following:

1. The eye attempts to keep the retinal flux roughly constant. So an increase in intensity causes a decrease in pupil area (*constriction*), while a decrease in intensity causes an increase in pupil area (*dilation*).
2. Pupil dilation involves a larger change in area compared to constriction for the same variation in intensity from a given state.

3. A finite time delay is involved as the pupil size varies with intensity, i.e. the process is not instantaneous.

However, a limitation of this model is that the pupillary response is assumed to be independent of other bodily functions. The reader is referred to (4) for a detailed analysis, where the dynamic response of retinal cells is coupled with pupillary reflex.

Note that τ, α and γ are the three independent parameters in system (2.1). However, the work in (6) did not provide a range of values for the same. The authors of (7) derived a numerical expression for (2.1) based on measured data,

$$\frac{dg}{dA}\frac{dA}{dt} + 2.3026.g(A) = -0.45 \ln \frac{I(t-0.18)A(t-0.18)}{5.02\text{x}10^{-5}}, \tag{2.2}$$

where area A is in the units of mm^2, intensity I is in lumens/mm^2, time t is in seconds and

$$g(A) = \tanh^{-1}\left(\frac{2\sqrt{\frac{A}{\pi}} - 4.9}{3}\right). \tag{2.3}$$

Notice that the range of the $tanh^{-1}$ function being $(-1, 1)$ places restrictions on the pupil area A as

$$2.84 < A < 49, \tag{2.4}$$

which closely characterises the physical limits of pupil expansion and contraction (7).

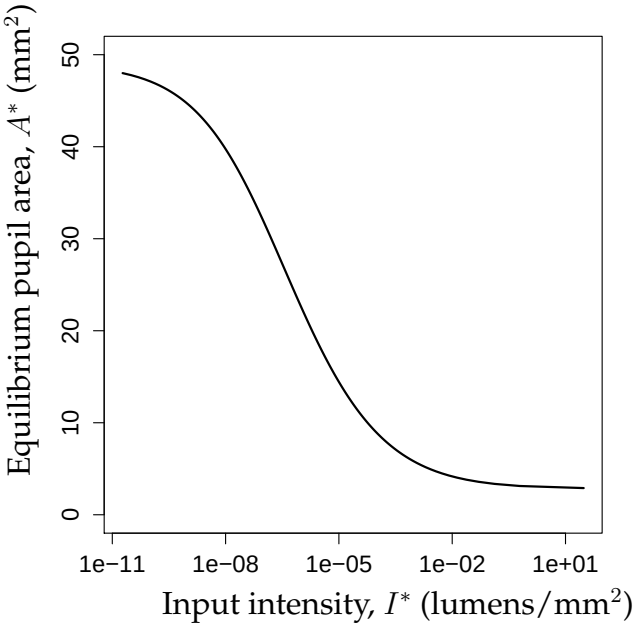

Figure 2.1: Variation of equilibrium pupil area with input intensity. Note the monotonicity, indicating a unique A^* for every I^*, for a given set of parameter values. We used $\alpha = 2.303/\sec, \gamma = -0.45/\sec, \tau = 0.18\sec$.

The equilibrium point of system (2.1) is obtained by putting $\frac{dA(t)}{dt} = 0$ to get

$$\alpha g(A^*) = \gamma \ln \frac{I^* A^*}{\hat{I}\hat{A}},$$

which defines the steady state area A^* for a steady state intensity I^*. Note that this point is unique (Figure 2.1), and dependent on values of parameters α and γ. To linearise the system (2.1), assume a small perturbation in the pupil area as

$$A(t) = A^* + y(t).$$

This gives

$$\alpha^{-1}\frac{dy(t)}{dt} + y(t) = Gy(t-\tau), \tag{2.5}$$

where gain $G = \frac{\gamma}{\alpha\beta A^*}$ and $\beta = \frac{dg}{dA}\Big|_{A=A^*}$. Note that $G < 0$, that is, γ and β take opposite signs to maintain negative feedback.

Now consider an input intensity $I(t) = I^* + x(t)$ causing a change in area as $A(t) = A^* + y(t)$, where $x(t)$ and $y(t)$ are incremental. Putting this into (2.1), we

get

$$\beta\frac{dy(t)}{dt} + \alpha\beta y(t) = \gamma\frac{y(t-\tau)}{A^*} + \gamma\frac{x(t-\tau)}{I^*}, \tag{2.6}$$

which is the linearised input-output model. Taking the Laplace Transform and rearranging terms gives

$$\frac{Y(s)}{X(s)} = K\frac{\alpha G e^{-s\tau}/(s+\alpha)}{1-\alpha G e^{-s\tau}/(s+\alpha)},$$

where $K = A^*/I^*$ and $G = \frac{\gamma}{\alpha\beta A^*}$. Again, note that $G < 0$ for negative feedback. Thus,

$$\frac{Y(s)}{X(s)} = H(s) = -K\frac{P(s)}{1+P(s)}, \tag{2.7}$$

where $P(s) = -\alpha G e^{-s\tau}/(s+\alpha)$ is the open loop transfer function. This constitutes a transfer function model as shown in Figure 2.2. We find that the neural delay is not part of the feedback, but is intrinsic to the pupillary response.

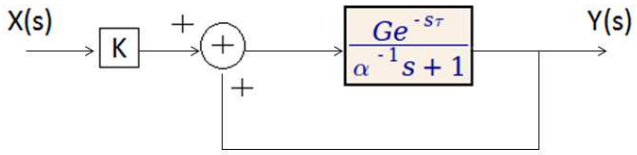

Figure 2.2: Block diagram for the linearised pupillary reflex model. Observe that the neural delay is intrinsic to the response, and not part of the feedback. Also, $G < 0$ constitutes negative feedback.

In the following chapter we carry out a systematic local stability analysis of the pupillary reflex model.

CHAPTER 3

Local Stability Analysis

In this chapter, we obtain conditions on parameter values for the pupillary reflex model to maintain local stability. For our analysis of the linearised Longtin-Milton equation (2.5), we derive these conditions algebraically, and with the help of Nyquist plots.

Notice that (2.5) can be expressed in the form

$$\frac{dy(t)}{dt} = -ay(t) - by(t-\tau), \tag{3.1}$$

where $a = \alpha$, $b = -\alpha G = -\frac{\gamma}{\beta A^*}$, and $\beta = \frac{dg}{dA}\Big|_{A=A^*}$. Note that $a, b, \tau > 0$ and A^* is the equilibrium pupil area. Substituting $y(t) = e^{\lambda t}$ gives the corresponding characteristic equation,

$$\lambda + a + be^{-\lambda\tau} = 0, \tag{3.2}$$

where $\lambda = \sigma + j\omega$. At the crossover between the regions of local stability and instability, the eigenvalues become purely imaginary, so $\sigma = 0$ and $\omega = \omega_0$. We now have

$$j\omega_0 + a + b\cos(\omega_0\tau) - jb\sin(\omega_0\tau) = 0.$$

Equating the real and imaginary parts to zero gives

$$\alpha + b\cos(\omega_0\tau) = 0, \tag{3.3}$$

$$\omega_0 - b\sin(\omega_0\tau) = 0. \tag{3.4}$$

Simplifying, we obtain

$$\omega_0 = \sqrt{b^2 - a^2} = \frac{1}{\tau}\cos^{-1}\left(-\frac{a}{b}\right). \tag{3.5}$$

The above equation gives us the condition for *marginal stability*. Under the assumption that larger time delays can destabilise the associated system, the nec-

essary and sufficient condition condition for local stability is

$$\tau\sqrt{b^2-a^2} < \cos^{-1}\left(-\frac{a}{b}\right).$$

Observe that $\tau\sqrt{b^2-a^2} < b\tau$ and $\frac{\pi}{2} < \cos^{-1}\left(-\frac{a}{b}\right)$. Thus,

$$b\tau < \frac{\pi}{2}$$

becomes a sufficient condition for local stability.

The above conditions for stability are demonstrated with the help of the *Nyquist Stability Criterion*. We construct the Nyquist contour that encircles the right half plane, and the corresponding Nyquist plot for the function

$$H(s) = s + a + be^{-s\tau},$$

for different parametric values of a, b and τ. The Nyquist plot of $H(s)$, for a stable system, should not encircle the origin. Observe that

$$min(real(H(s))) = a - b.$$

Thus,

$$a \geq b,$$

is another sufficient condition for local stability, since the Nyquist plot will never encircle the origin if it is satisfied.

Thus, we have shown that

$$a \geq b, \tag{3.6}$$

and

$$b\tau < \pi/2 \tag{3.7}$$

are *sufficient conditions* for local stability, and

$$\tau\sqrt{b^2-a^2} < \cos^{-1}\left(-\frac{a}{b}\right) \tag{3.8}$$

is the *necessary and sufficient condition* for local stability. We now apply these

conditions to derive the corresponding results for the pupillary reflex model.

Sufficient conditions for local stability

By substituting values from the linearised pupillary reflex model (3.1) into the sufficient condition for stability (3.6), we obtain $\alpha \geq -\alpha G$, or

$$G \geq -1. \tag{3.9}$$

If this is the case, the coefficient of $y(t)$ in (3.1) is greater than that of the delay term $y(t-\tau)$. Tuning the gain to satisfy (3.9) is the easiest method of guaranteeing local stability *irrespective of the neural delay*.

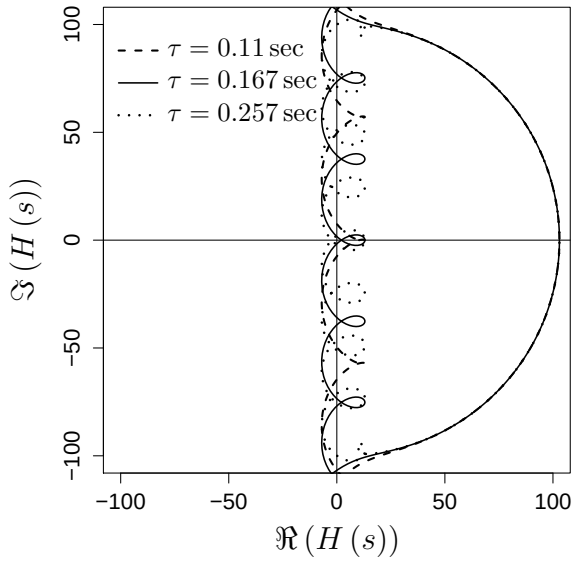

Figure 3.1: Keeping $a = 3/\,\text{sec}$ and $b = 10\,\text{sec}$ constant in the characteristic equation (3.2), we vary the delay parameter τ to analyse how the Nyquist plot reflects the transition into instability. To ensure stability according to the Nyquist criterion, the plot should not encircle the origin.

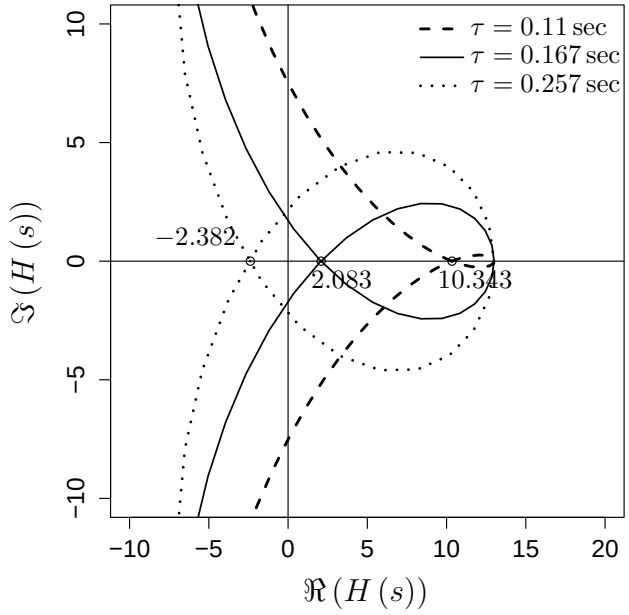

Figure 3.2: For $\tau = 0.11\,\text{sec}$, $b\tau < \frac{\pi}{2}$. The only points on the real axis enclosed by the plot lie in $(a, a+b)$. Since $a, b > 0$, the plot does not encircle the origin. For $\tau = 0.167\,\text{sec}$, $b\tau > \frac{\pi}{2}$. The plot still does not encircle the origin, ensuring stability. Note that $\tau\sqrt{b^2 - a^2} < \cos^{-1}\left(-\frac{a}{b}\right)$. For $\tau = 0.257\,\text{sec}$, $b\tau > \frac{\pi}{2}$ and $\tau\sqrt{b^2 - a^2} > \cos^{-1}\left(-\frac{a}{b}\right)$. The plot encircles the origin, denoting the transition to instability. This confirms our assumption that for a particular value of a and b, large time delays can destabilise the associated system.

Using the other sufficient condition for stability (3.7) gives

$$-\alpha G\tau < \frac{\pi}{2}, \tag{3.10}$$

which, by substituting for $G = \frac{\gamma}{\alpha g'(A^*)A^*}$, can be expressed as

$$-\gamma\tau < \frac{\pi}{2} g'(A^*)A^*. \tag{3.11}$$

This indicates that the known equilibrium condition A^* can be used to restrict the product of the neural constant γ and neural delay τ to ensure local stability.

Substituting for the parameters γ and α from the numerical model (2.2), the

restrictions on A from (2.4) cause the limits of G to be

$$-0.21 < G < -7\text{x}10^{-5},$$

which ensures stability of system (2.2) according to (3.9).

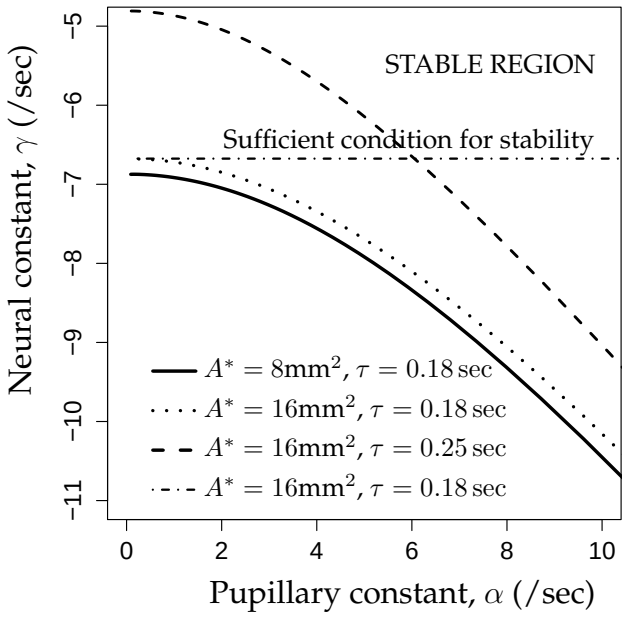

Figure 3.3: Variation in the range of allowed values for α and γ at different neural delays and equilibria, to maintain stability. From (3.12), an increase in τ further restricts this range. Note that stability is maintained for values *above* the constructed curves.

Necessary and sufficient condition for local stability

Substituting values from the linearised pupillary reflex model (3.1) into the condition (3.8) yields

$$\alpha\tau\sqrt{G^2 - 1} < \cos^{-1}\left(\frac{1}{G}\right),$$

which is the necessary and sufficient condition for local stability about (I^*, A^*). Expressing this in terms of system parameters τ, α and γ and using $\beta = g'(A^*)$, we get

$$\alpha\tau\sqrt{\left(\frac{\gamma}{\alpha\beta A^*}\right)^2 - 1} < \cos^{-1}\left(\frac{\alpha\beta A^*}{\gamma}\right). \tag{3.12}$$

This condition is a complicated mathematical relationship compared to either of the sufficient conditions (3.9)(3.11) and is clearly not easy to satisfy from a

design point of view. However it does give more leeway in terms of allowed parameter values to maintain local stability.

The implications of the above conditions are explored by plotting stability charts.

Stability charts

Conditions for local stability have been derived with respect to three independent system parameters. Stability charts provide an opportunity to understand the trade-offs between parameter values so as to keep the associated system stable; the reader is referred to Figures 3.3, 3.4 and 3.5.

We will show in a later chapter that the stability curves represent the condition for undergoing a *Hopf bifurcation*. Notice from the stability charts that the independent parameters α, γ and τ play the major role in influencing local stability, and not the equilibrium pupil area A^*. We can reduce the number of parameters affecting local stability to two by ensuring that the sufficient condition (3.11)

$$-\gamma\tau < \frac{\pi}{2} g'(A^*)A^*,$$

is satisfied. Thus, α could be chosen purely with the aim of achieving a desired transient response, which is studied in the next chapter.

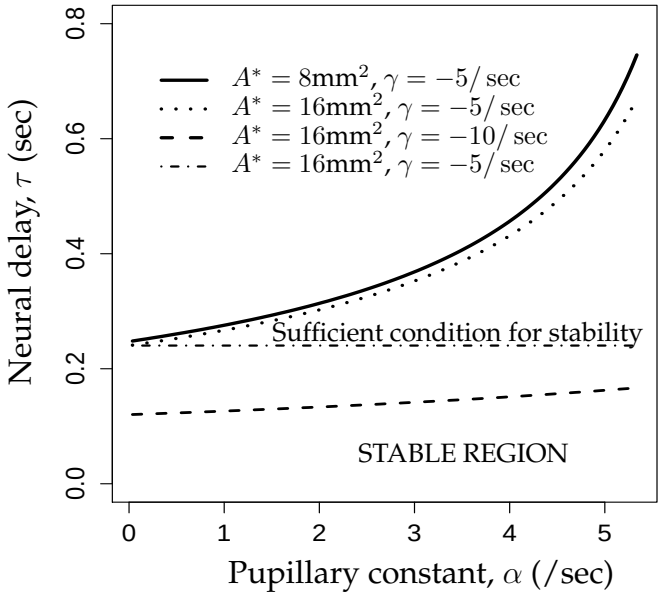

Figure 3.4: Variation in the range of allowed values for τ and α at different neural constants and equilibria, to maintain stability. An increase in $|\gamma|$ increases the coefficient of the delay term $y(t-\tau)$ in (3.1), restricting this range and pushing the system (2.1) to instability. Note that stability is maintained for values *below* the curves.

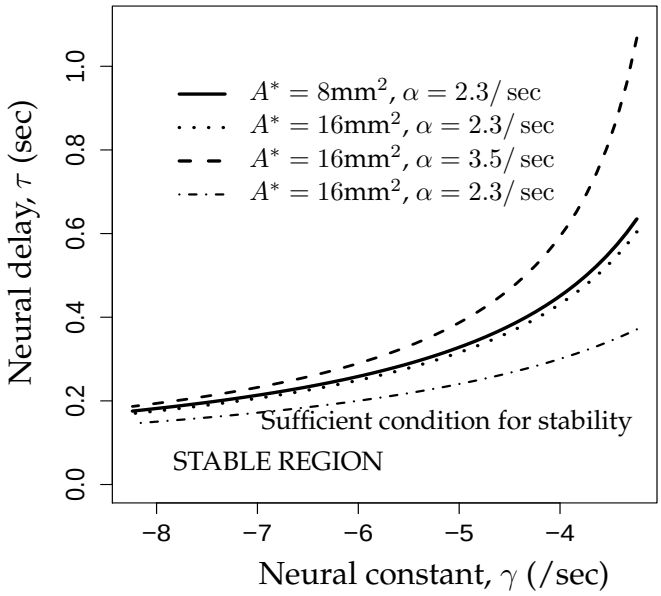

Figure 3.5: Variation in the range of allowed values for τ and γ for different pupillary constants and equilibria, to maintain stability. Being the coefficient of the $y(t)$ term in (3.1), an increase in α pushes the system (2.1) further into stability. Note that stability is maintained for values *below* the curves.

CHAPTER 4

Local Rate of Convergence

Rate of convergence refers to how quickly a dynamical system settles to its new state, when perturbed by a small change in the input about its equilibrium point. In our case, a fractional change in the ambient intensity of light causes the pupil area to change incrementally. We analyse, in the region of locally stability, the rate at which the pupil area settles to its final value as a function of system parameters. Parameter values determine if the pupillary response is *underdamped*, *critically damped* or *overdamped*.

Consider a small step input $I^* + u(t)$ triggering a response $A^* + y(t)$, which is found using the linearised model (2.6). Settling time t_s is the time taken for the response to achieve a state such that $\forall t > t_s$,

$$|y(t) - y_\infty| < p\% * |y_\infty - A^*| \,.$$

In other words, the output $y(t)$ gets bound within a certain band $(p\%)$ around the final value y_∞. In our case, we choose $p = 5$. We now define *local rate of convergence* as

$$RoC = 1/t_s.$$

For our analysis, the linear system under consideration is (3.1)

$$\frac{dy(t)}{dt} = -ay(t) - by(t-\tau),$$

whose characteristic equation takes the form (3.2)

$$\lambda + a + be^{-\lambda\tau} = 0,$$

where $\lambda = \sigma + j\omega$. For an overdamped response, $\sigma < 0$ and there are no

sinusiodal components, so $\omega = 0$. Therefore, $\lambda = \sigma$, and

$$\sigma + a + be^{-\sigma\tau} = 0.$$

For the above equation to have a solution in $\sigma < 0$, the minima of $f(\sigma) = \sigma + a + be^{-\sigma\tau}$ must be lesser than zero. The derivative of $f(\sigma)$ is

$$f^{'}(\sigma) = 1 - b\tau e^{-\sigma\tau},$$

and it becomes zero at $\sigma_{min} = ln(b\tau)/\tau$. Under the assumption that $min(f(\sigma)) < 0$, it can be readily shown that

$$b\tau < e^{-a\tau-1}, \tag{4.1}$$

which is the necessary and sufficient condition for an overdamped response. We have plotted the different regions of overdamping, underdamping and instability in Figure 4.1. For the pupillary reflex model (3.1), the condition on parameters α, γ, τ from (4.1) is expressed as

$$\frac{\gamma\tau}{g'(A^*)A^*} < e^{-\alpha\tau-1}. \tag{4.2}$$

A sufficient condition for stability (3.11) derived earlier was found to be independent of the pupillary constant α. Comparing the above result (4.2) with (3.11) shows how the pupillary constant now influences damping within the region of local stability.

The reader is referred to Figures 4.2 and 4.3. We find that allowing the neural constant γ to vary can cause the pupillary response to swing between being overdamped, underdamped and even unstable regardless of the other parameter values. However, by fixing γ and the time delay τ, we can guarantee that the response remains either overdamped or underdamped irrespective of the value of the pupillary constant α.

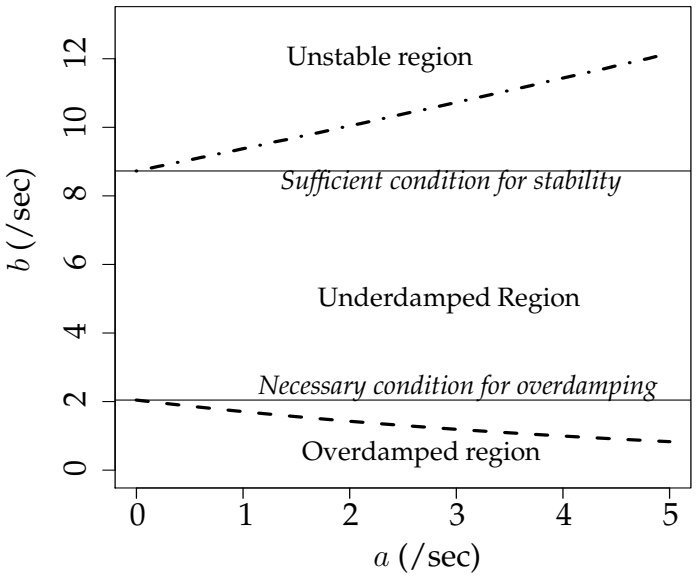

Figure 4.1: Variation of transient response of $\frac{dy(t)}{dt} = -ay(t) - by(t-\tau)$ with values of a and b. Note how b governs stability and the nature of damping to a larger extent than a. Choosing b appropriately can guarantee an underdamped response for all $a > 0$. We used $\tau = 0.18\,\text{sec}$.

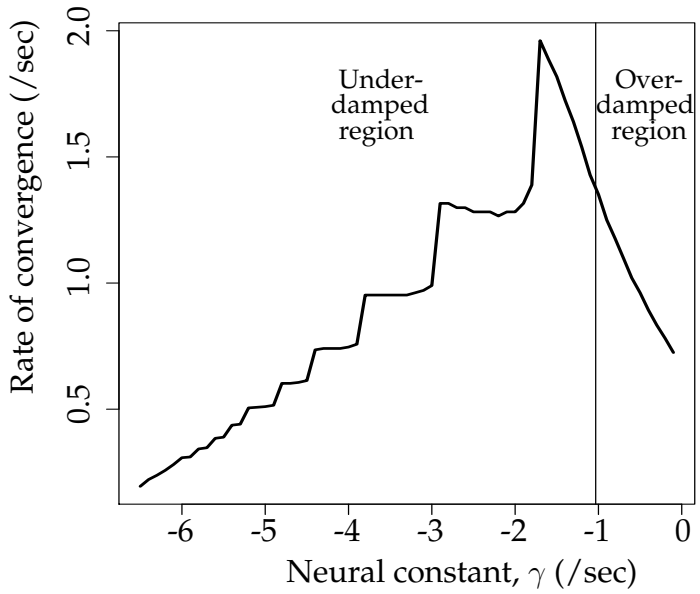

Figure 4.2: Rate of convergence of the pupillary reflex model (3.1) as a function of the neural constant γ. An increase in $|\gamma|$ causes the pupil area to settle faster, and makes the response underdamped. However, a drastic drop in the rate is noted as the initial output peak of $y(t)$ goes beyond the $\pm 5\%$ range. We used equilibrium area $A^* = 16mm^2$, $\alpha = 2.303/\,\text{sec}$, $\tau = 0.18\,\text{sec}$.

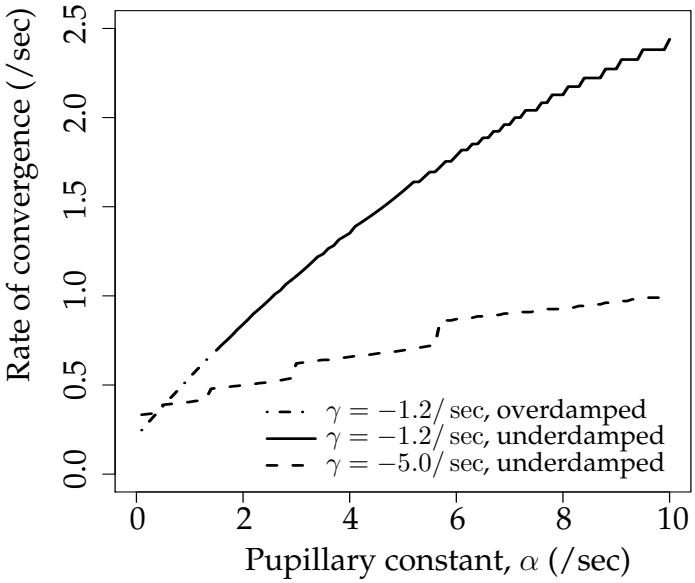

Figure 4.3: Rate of convergence of the pupillary reflex model (3.1) as a function of the pupillary constant α. Note that the response can vary from being underdamped to overdamped, or is always underdamped. $A^* = 16mm^2$, $\tau = 0.18\,\text{sec}$.

CHAPTER 5

Robustness

Dynamical systems from the real world, modelled mathematically, naturally come with certain *uncertainties*. These may take form in the model itself, or in the values of parameters used. A *robust* model is one that ensures stability and a desired level of performance even in the presence of these uncertainties. In this chapter, we analyse the robustness of the pupillary reflex model under consideration (2.1), as a function of parameter uncertainties.

The Vinnicombe metric (1) is used the measure the 'difference' between two closed loop transfer functions. This can be interpreted as the difference between the complementary sensitivity functions of the two systems under comparison. Consider the associated process functions P_1 and P_2. The Vinnicombe metric is defined as

$$d\left(P_1, P_2\right) = \sup_{\omega} \frac{\left|P_1\left(i\omega\right) - P_2\left(i\omega\right)\right|}{\sqrt{\left(1 + \left|P_1\left(i\omega\right)\right|^2\right)\left(1 + \left|P_2\left(i\omega\right)\right|^2\right)}},$$

where $d\left(P_1, P_2\right) \in [0, 1]$. We use the Vinnicombe metric as a robustness measure by comparing a model containing uncertainty with the one without. From (1), we apply the rule that if

$$d\left(P_1, P_2\right) < 1/3, \tag{5.1}$$

the model is reasonably robust. Hence, bounds on the uncertainty in any parameter can be found to ensure reasonable robustness.

The loop transfer function for the pupillary reflex model is given by (2.5)

$$P\left(s\right) = \frac{-\alpha G e^{-s\tau}}{s + \alpha},$$

where $G = \frac{\gamma}{\alpha\beta A^*}$, $\beta = \left.\frac{dg}{dA}\right|_{A=A^*}$ and A^* is the equilibrium pupil area. Let $P_1\left(s\right) = P(s)$ be the given function, and $P_2\left(s\right)$ be the function containing an uncertainty. We first assume that γ amd τ are known accurately and there exists an uncertainty in the pupillary constant α. Let $\alpha = \alpha_u$ in $P_2(s)$ and $\alpha = \alpha_c$

in $P_1(s)$. On fixing α_c and varying α_u, one can compute the Vinnicombe metric for all values of α_u in the region of local stability. Where $d\left(P_1, P_2\right)$ never exceeds $\frac{1}{3}$, the system is robust. A similar process is carried out for γ. The reader is referred to Figures 5.1 and 5.2, which offer guidelines to choose parameter values in the stable region to ensure robustness.

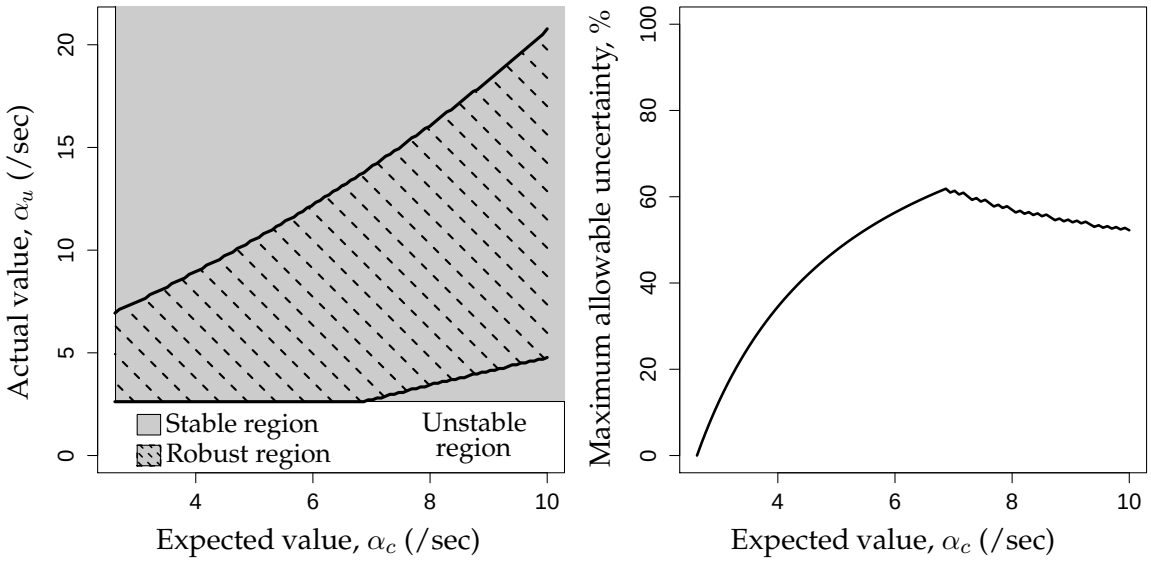

Figure 5.1: The allowed variations in pupillary constant α to ensure reasonable robustness according to the condition (5.1). $\alpha_c \in P_1(s)$, the process function and $\alpha_u \in P_2(s)$, the process function with uncertainty. Observe that as α_c approaches the limit for stability, the maximum allowable uncertainity to ensure robustness, drops to 0. $\gamma = -8/\sec$, $\tau = 0.18\sec$, $A^* = 16mm^2$.

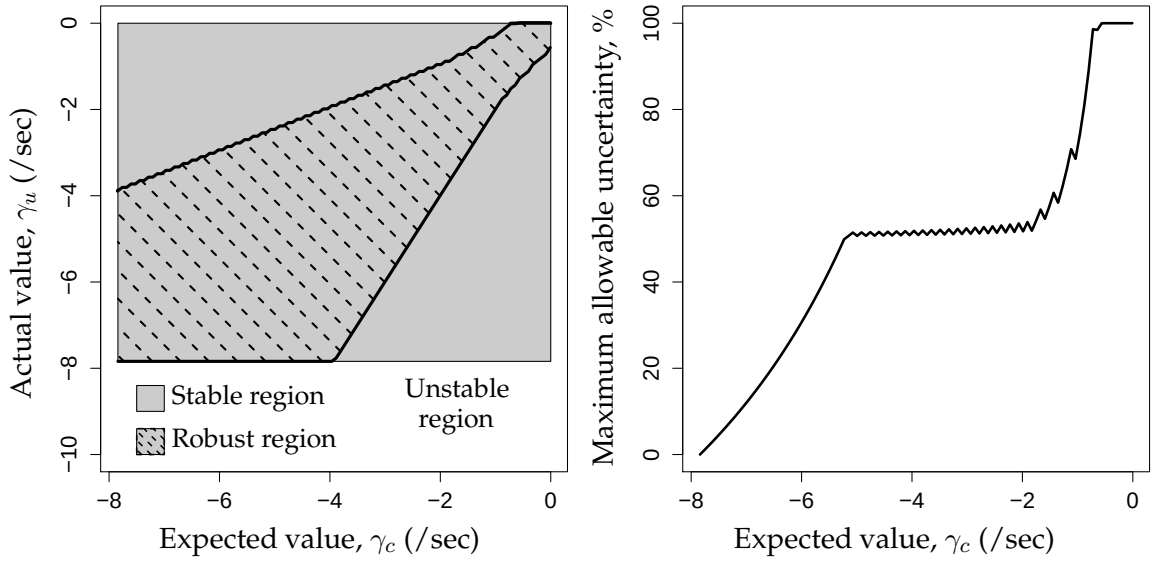

Figure 5.2: The allowed variations in neural constant γ to ensure reasonable robustness according to the condition (5.1). $\gamma_c \in P_1(s)$, the process function and $\gamma_u \in P_2(s)$, the process function with uncertainty. Observe that as γ_c approaches the limit for stablity, the maximum allowable uncertainity to ensure robustness, drops to 0. $\alpha = 2.303/\sec$, $\tau = 0.18\sec$, $A^* = 16mm^2$.

CHAPTER 6

Local Bifurcation Analysis

We have so far studied the behaviour of the pupillary reflex model within its range of local stability. In this chapter, a systematic local bifurcation analysis is carried out. We prove that the loss of local stability is induced via Hopf bifurcations. The bifurcation points are then analytically characterised, including the types of Hopf induced, and the stability of the bifurcating solutions.

6.1 Existence of Hopf Bifurcations

Consider a characteristic equation of the form

$$f(\lambda, K_1, K_2, ..., K_n) = 0,$$

where $\lambda = \sigma + j\omega$ is a complex variable and K_i's are the system parameters. The transversality condition states that a local *Hopf bifurcation* is induced with respect to a parameter K_i if

$$\rho'(0) = Re\left(\frac{d\lambda}{dK_i}\right)\Big|_{K_i=K_{i,c}} \neq 0 \tag{6.1}$$

where $K_{i,c}$ is the critical value of the parameter K_i satisfying the Hopf condition (5). Choosing $K_i = K_{i,c} + \mu$, where μ is called the bifurcation parameter, gives rise to limit cycle oscillations. Note that at $K_i = K_{i,c}$ the eigenvalues lie on the imaginary axis, and so $\sigma = 0$ and $\lambda = j\omega_0$.

The characteristic equation we consider is

$$\lambda + a + be^{-\lambda\tau} = 0,$$

where the critical values of the parameters a, b, τ are obtained from (3.5). Dif-

ferentiating with respect to a gives

$$\frac{d\lambda}{da} = \frac{1}{b\tau e^{-\lambda\tau} - 1}.$$

Dividing the right hand side into real and imaginary parts and substituting values using (3.5), we obtain

$$Re\left(\frac{d\lambda}{da}\right)\Big|_{a=a_c} = \frac{-(a_c\tau+1)}{(a_c\tau+1)^2 + \left\{\cos^{-1}\left(-\frac{a_c}{b}\right)\right\}^2},$$

where a_c is the critical value of the parameter a. Following a similar procedure for b and τ yields:

$$Re\left(\frac{d\lambda}{db}\right)\Big|_{b=b_c} = \frac{b_c\tau + a/b_c}{(a\tau+1)^2 + \left\{\cos^{-1}\left(-\frac{a}{b_c}\right)\right\}^2},$$

$$Re\left(\frac{d\lambda}{d\tau}\right)\Big|_{\tau=\tau_c} = \frac{\left\{\frac{1}{\tau_c}\cos^{-1}\left(-\frac{a}{b}\right)\right\}^2}{(a\tau_c+1)^2 + \left\{\cos^{-1}\left(-\frac{a}{b}\right)\right\}^2}.$$

We now substitute in these expressions, parameters from the pupillary reflex model (2.1). The critical values of α, γ and τ are obtained from the condition for marginal stability, (3.5)

$$\alpha\tau\sqrt{\left(\frac{\gamma}{\alpha\beta A^*}\right)^2 - 1} = \cos^{-1}\left(\frac{\alpha\beta A^*}{\gamma}\right).$$

This gives

$$Re\left(\frac{d\lambda}{d\alpha}\right)\Big|_{\alpha=\alpha_c} = \frac{-(\alpha_c\tau+1)}{(\alpha_c\tau+1)^2 + \left\{\cos^{-1}\left(\frac{\beta A^*\alpha_c}{\gamma}\right)\right\}^2} < 0, \tag{6.2}$$

since $\alpha_c, \tau > 0$,

$$Re\left(\frac{d\lambda}{d\gamma}\right)\Big|_{\gamma=\gamma_c} = \frac{(1/\beta A^*)}{(\alpha\tau+1)^2 + \left\{\cos^{-1}\left(\frac{\beta A^*\alpha}{\gamma_c}\right)\right\}^2} > 0, \tag{6.3}$$

since $\beta, A^* > 0$, and

$$Re\left(\frac{d\lambda}{d\tau}\right)\Big|_{\tau=\tau_c} = \frac{\left\{\frac{1}{\tau_c}\cos^{-1}\left(\frac{\beta A^*\alpha^2}{\gamma}\right)\right\}^2}{(\alpha\tau_c+1)^2+\left\{\cos^{-1}\left(\frac{\beta A^*\alpha}{\gamma}\right)\right\}^2} > 0. \tag{6.4}$$

Thus, a loss in stability of the pupillary reflex model due to any parameter occurs via a Hopf bifurcation. The pupillary response undergoes limit cycle oscillations when it transitions into instability. This behaviour is now analytically characterised.

6.2 Analytical Characterization: Stability and Periodicity of Solutions

Note that linearised pupillary reflex model (3.1) is a special case of the form

$$\frac{d}{dt}x(t) = \kappa f(x(t), x(t-\tau)), \tag{6.5}$$

where τ is a constant delay. According to the normal form of the Hopf bifurcation, the linear, quadratic, and cubic terms are required to characterise the Hopf. Define $u(t) = x(t) - x^*$, $y \equiv x(t-\tau)$ and expand (6.5) as

$$\begin{aligned}\frac{d}{dt}u(t) &= \kappa\xi_x u(t) + \kappa\xi_y u(t-\tau) + \kappa\xi_{xx}u^2(t) \\ &\quad + \kappa\xi_{yy}u^2(t-\tau) + \kappa\xi_{xxx}u^3(t) \\ &\quad + \kappa\xi_{xxy}u^2(t)u(t-\tau) + \kappa\xi_{xyy}u(t)u^2(t-\tau) \\ &\quad + \kappa\xi_{yyy}u^3(t-\tau) + O(u^4),\end{aligned} \tag{6.6}$$

where

$$\begin{aligned}\xi_x &= f_x^*, \xi_y = f_y^*, \xi_{xx} = \frac{1}{2}f_{xx}^*, \\ \xi_{xy} &= f_{xy}^*, \xi_{yy} = \frac{1}{2}f_{yy}^*, \xi_{xxx} = \frac{1}{6}f_{xxx}^*, \\ \xi_{xxy} &= \frac{1}{2}f_{xxy}^*, \xi_{xyy} = \frac{1}{2}f_{xyy}^*, \xi_{yyy} = \frac{1}{6}f_{yyy}^*.\end{aligned}$$

f^* indicates calculation of coefficients at equilibrium, and the system parameters take values satisfying the Hopf condition (5).

For the pupillary reflex model, (2.1)

$$\frac{dA}{dt} = -\frac{\alpha g(A)}{g'(A)} + \frac{\gamma}{g'(A)} \ln \frac{I(t-\tau)A(t-\tau)}{\hat{I}\hat{A}},$$

the function $g(A)$ is defined as (2.2)

$$g(A) = \tanh^{-1}\left(\frac{2\sqrt{\frac{A}{\pi}} - 4.9}{3}\right).$$

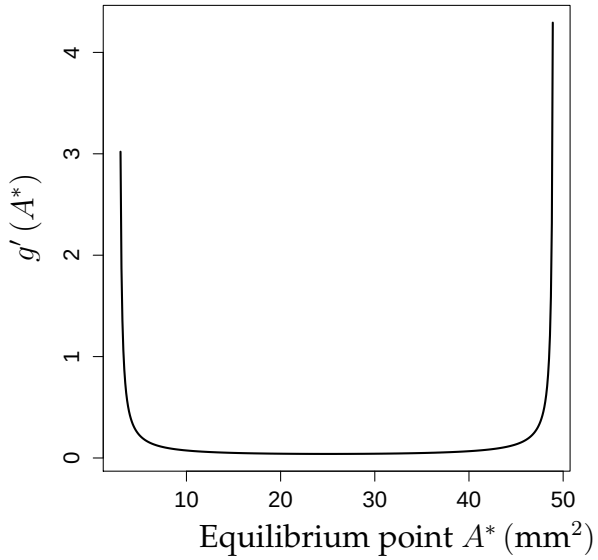

Figure 6.1: It is illustrated that $\beta = g'(A^*)$ can be assumed to be a constant in the neighbourhood of A^*, if the equilibrium point is chosen appropriately.

This is plotted in Figure (6.1). Clearly, $g'(A)$ remains approximately constant, except near the lower and upper limits of A. Thus, by choosing the equilibrium area A^* within this range, we can assume that the higher order derivatives of $g'(A)$ go to zero. If this assumption is not made, the evaluation of the quadratic and cubic coefficients in (6.7) would become extremely complex.

The coefficients for pupillary response, taking equilibrium area as A^* and

$\beta = g'(A^*) \approx$ constant, come out to be

$$\xi_x = -\alpha, \xi_y = \frac{\gamma}{\beta A^*}, \xi_{xx} = 0, \xi_{xy} = 0, \xi_{yy} = -\frac{\gamma}{2\beta(A^*)^2},$$
$$\xi_{xxx} = 0, \xi_{xxy} = 0, \xi_{xyy} = 0, \xi_{yyy} = \frac{\gamma}{3\beta(A^*)^3}.$$

Recall that the characteristic equation for pupillary reflex is (3.2)

$$\lambda + a + be^{-\lambda\tau} = 0,$$

where $\lambda = j\omega$ at the Hopf condition, and

$$\omega_0 = \frac{1}{\tau}\cos^{-1}\left(-\frac{a}{b}\right).$$

Define

$$\rho'(0) = \Re\left(\frac{d\lambda}{dK_i}\right)\Bigg|_{K_i=K_{i,c}},$$

where $K_i = K_{i,c}$ is the value of system parameter K_i at the Hopf condition and

$$\omega'(0) = \Im\left(\frac{d\lambda}{dK_i}\right)\Bigg|_{K_i=K_{i,c}}.$$

Following the work of (5), we perform the necessary calculations to analytically characterize the bifurcation points of the system (2.1). Consider the following autonomous delay differential system, of which the pupillary reflex model is a specific case:

$$\frac{d}{dt}u(t) = \mathcal{L}_\mu u_t + \mathcal{F}(u_t, \mu), \tag{6.7}$$

where $t > 0$, $\mu \in \mathbb{R}$, and for $\tau > 0$,

$$u_t(\theta) = u(t+\theta) \quad u : [-\tau, 0] \to \mathbb{R} \quad \theta \in [-\tau, 0].$$

$\mathcal{L}_\mu$ is a one-parameter family of continuous linear bounded operators defined as $\mathcal{L}_\mu : C[-\tau, 0] \to \mathbb{R}$. The operator $\mathcal{F}(u_t, \mu) : C[-\tau, 0] \to \mathbb{R}$ contains the nonlinear terms. Further, assume that $\mathcal{F}(u_t, \mu)$ is analytic and that $\mathcal{F}$ and $\mathcal{L}_\mu$ depend analytically on the bifurcation parameter μ for small $|\mu|$. The objective now is

to cast (6.7) into the form

$$\frac{d}{dt}u_t = A(\mu)u_t + Ru_t, \tag{6.8}$$

which has u_t rather than both u and u_t. First transform the linear problem $\frac{d}{dt}u(t) = \mathcal{L}_\mu u_t$. By the Reisz Representation Theorem, there exists an $n \times n$ matrix-valued function $\eta(\cdot, \mu) : [-\tau, 0] \to \mathbb{R}^{n^2}$, such that each component of η has bounded variation and for all $\phi \in C[-\tau, 0]$,

$$\mathcal{L}_\mu \phi = \int_{-\tau}^{0} d\eta(\theta, \mu)\phi(\theta).$$

In particular

$$\mathcal{L}_\mu u_t = \int_{-\tau}^{0} d\eta(\theta, \mu)u(t + \theta). \tag{6.9}$$

Observe that

$$d\eta(\theta, \mu) = (\kappa\xi_x\delta(\theta) + \kappa\xi_y\delta(\theta + \tau))d\theta,$$

where $\delta(\theta)$ is the Dirac delta function, would satisfy (6.9).

For $\phi \in C^1[-\tau, 0]$, define

$$A(\mu)\phi(\theta) = \begin{cases} \frac{d\phi(\theta)}{d\theta} & \theta \in [-\tau, 0] \\ \int_{-\tau}^{0} d\eta(s, \mu)\phi(s) \equiv \mathcal{L}_\mu\phi & \theta = 0, \end{cases}$$

and

$$R\phi(\theta) = \begin{cases} 0 & \theta \in [-\tau, 0] \\ \mathcal{F}(\phi, \mu) & \theta = 0. \end{cases}$$

Then, as $\frac{du_t}{d\theta} \equiv \frac{du_t}{dt}$, system (6.7) becomes (6.8) as desired.

The bifurcating periodic solutions $u(t, \mu(\epsilon))$ of (6.7) (where $\epsilon \geq 0$ is a small parameter) have amplitude $O(\epsilon)$, period $P(\epsilon)$ and non-zero Floquet exponent

$\beta(\epsilon)$, where μ, P and β have the following (convergent) expansions:

$$\begin{aligned}\mu &= \mu_2\epsilon^2 + \mu_4\epsilon^4 + \cdots \\ P &= \frac{2\pi}{\omega_0}(1 + T_2\epsilon^2 + T_4\epsilon^4 + \cdots) \\ \beta &= \beta_2\epsilon^2 + \beta_4\epsilon^4 + \cdots .\end{aligned}$$

The signs of μ_2 and β_2 determine the direction of bifurcation and the stability of $u(t, \mu(\epsilon))$ respectively. We need to compute the expressions at $\mu = 0$, hence we set $\mu = 0$ in the following. Let $q(\theta)$ be the eigenfunction for $A(0)$ corresponding to $\lambda(0)$, namely

$$A(0)q(\theta) = j\omega_0 q(\theta),$$

and define the adjoint operator $A^*(0)$ as

$$A^*(0)\alpha(s) = \begin{cases} -\frac{d\alpha(s)}{ds} & s \in (0, \tau] \\ \int_{-\tau}^{0} d\eta^T(t, 0)\alpha(-t) & s = 0, \end{cases}$$

where η^T denotes the transpose of η.

Note that the domains of A and A^* are $C^1[-\tau, 0]$ and $C^1[0, \tau]$. As

$$Aq(\theta) = \lambda(0)q(\theta),$$

$\lambda(0)$ is an eigenvalue for A^*, and

$$A^*q^* = -j\omega_0 q^*$$

for some non-zero vector q^*. For $\phi \in C[-\tau, 0]$ and $\psi \in C[0, \tau]$, define an inner product

$$\langle \psi, \phi \rangle = \bar{\psi}(0).\phi(0) - \int_{\theta=-\tau}^{0} \int_{\zeta=0}^{\theta} \bar{\psi}^T(\zeta - \theta)d\eta(\theta)\phi(\zeta)d\zeta, \tag{6.10}$$

where $a.b$ means $\sum_{i=1}^{n} a_i b_i$. Then, $\langle \psi, A\phi \rangle = \langle A^*\psi, \phi \rangle$ for $\phi \in \text{Dom}(A)$, $\psi \in \text{Dom}(A^*)$. Let $q(\theta) = e^{j\omega_0\theta}$ and $q^*(s) = De^{j\omega_0 s}$ be the eigenvectors for A and A^*

corresponding to the eigenvalues $+j\omega_0$ and $-j\omega_0$. With

$$D = \frac{1}{1 + \tau\kappa\xi_y e^{j\omega_0\tau}},$$

we get $\langle q^*, q\rangle = 1$ and $\langle q^*, \bar{q}\rangle = 0$. Using (6.10), we first confirm $\langle q^*, q\rangle = 1$,

$$\begin{aligned}\langle q^*, q\rangle &= \bar{D} - \bar{D}\int_{\theta=-\tau}^{0} \theta e^{j\omega_0\theta}(\kappa\xi_x\delta(\theta) + \kappa\xi_y\delta(\theta+\tau))d\theta \\ &= \bar{D} + \bar{D}\kappa\tau\xi_y e^{-j\omega_0\tau} \\ &= 1.\end{aligned}$$

Similarly we can show that $\langle q^*, q\rangle = 0$. Again, using (6.10), we get

$$\begin{aligned}\langle q^*, \bar{q}\rangle &= \bar{D} + \frac{\bar{D}\kappa}{2j\omega_0}\int_{\theta=-\tau}^{0} (e^{-j\omega_0\theta} - e^{j\omega_0\theta})(\xi_x\delta(\theta) \\ &\quad + \xi_y\delta(\theta+\tau))d\theta \\ &= \bar{D} + \frac{\bar{D}\kappa}{2j\omega_0}\xi_y(e^{j\omega_0\tau} - e^{-j\omega_0\tau}) \\ &= 0.\end{aligned}$$

For u_t, a solution of (6.8) at $\mu = 0$, define

$$\begin{aligned}z(t) &= \langle q^*, u_t\rangle \\ w(t,\theta) &= u_t(\theta) - 2\Re z(t)q(\theta).\end{aligned}$$

Then, on the manifold C_0, $w(t,\theta) = w(z(t), \bar{z}(t), \theta)$ where

$$w(z, \bar{z}, \theta) = w_{20}(\theta)\frac{z^2}{2} + w_{11}(\theta)z\bar{z} + w_{02}(\theta)\frac{\bar{z}^2}{2} + \cdots . \tag{6.11}$$

In effect, z and $\bar{z}$ are local coordinates for C_0 in C in the directions of q and q^*, respectively. Note that w is real if u_t is real and we deal only with real solutions. The existence of the centre manifold C_0 enables the reduction of (6.8) to an ordinary differential equation for a single complex variable on C_0. At

$\mu = 0$, this is

$$\begin{aligned} z'(t) &= \langle q^*, Au_t + Ru_t \rangle \\ &= j\omega_0 z(t) + \bar{q}^*(0).\mathcal{F}(w(z,\bar{z},\theta) + 2\Re\{z(t)q(\theta)\}) \\ &= j\omega_0 z(t) + \bar{q}^*(0).\mathcal{F}_0(z,\bar{z}), \end{aligned} \tag{6.12}$$

which is written in abbreviated form as

$$z'(t) = j\omega_0 z(t) + g(z,\bar{z}). \tag{6.13}$$

The next objective is to expand g in the powers of z and $\bar{z}$. However, we also have to determine the coefficients of $w_{ij}(\theta)$ in (6.11). Once the $w_{ij}(\theta)$ have been determined, the differential equation (6.12) for z would be explicit [as abbreviated in (6.13)]. Expanding the function $g(z,\bar{z})$ in powers of z and $\bar{z}$ we have

$$\begin{aligned} g(z,\bar{z}) &= \bar{q}^*(0).\mathcal{F}_0(z,\bar{z}) \\ &= g_{20}\frac{z^2}{2} + g_{11}z\bar{z} + g_{02}\frac{\bar{z}^2}{2} + g_{21}\frac{z^2\bar{z}}{2} + \cdots . \end{aligned}$$

Following (5), we write

$$w' = u_t' - z'q - \bar{z}'\bar{q},$$

and using (6.8) and (6.13) we obtain

$$w' = \begin{cases} Aw - 2\Re\bar{q}^*(0).\mathcal{F}_0 q(\theta) & \theta \in [-\tau, 0) \\ Aw - 2\Re\bar{q}^*(0).\mathcal{F}_0 q(0) + \mathcal{F}_0 & \theta = 0, \end{cases} \tag{6.14}$$

which is rewritten as

$$w' = Aw + H(z,\bar{z},\theta) \tag{6.15}$$

using (6.12), where

$$H(z,\bar{z},\theta) = H_{20}(\theta)\frac{z^2}{2} + H_{11}(\theta)z\bar{z} + H_{02}(\theta)\frac{\bar{z}^2}{2} + \cdots . \tag{6.16}$$

Now, on C_0, near the origin

$$w' = w_z z' + w_{\bar{z}} \bar{z}'.$$

Using (6.11) and (6.13) to replace w_z, z'(and their conjugates by their power series expansion) and equating with (6.15), we get

$$\begin{aligned}
(2j\omega_0 - A)w_{20}(\theta) &= H_{20}(\theta) \\
-Aw_{11}(\theta) &= H_{11}(\theta) \\
-(2j\omega_0 + A)w_{02}(\theta) &= H_{02}(\theta).
\end{aligned}$$

We start by observing

$$\begin{aligned}
u_t(\theta) &= w(z, \bar{z}, \theta) + zq(\theta) + \bar{z}\bar{q}(\theta) \\
&= w_{20}(\theta)\frac{z^2}{2} + w_{11}(\theta)z\bar{z} + w_{02}\frac{\bar{z}^2}{2} \\
&\quad + ze^{j\omega_0\theta} + \bar{z}e^{-j\omega_0\theta} + \cdots
\end{aligned}$$

from which we obtain $u_t(0)$ and $u_t(-\tau)$. We have actually looked ahead and as we will only be requiring the coefficients of $z^2, z\bar{z}, \bar{z}^2$ and $z^2\bar{z}$, we only keep these relevant terms in the following expansions:

$$\begin{aligned}
u_t^2(0) &= (w(z, \bar{z}, 0) + z + \bar{z})^2 \\
&= z^2 + \bar{z}^2 + 2z\bar{z} + z^2\bar{z}(2w_{11}(0) + w_{20}(0)) + \cdots .
\end{aligned}$$

$$\begin{aligned}
u_t^3(0) &= (w(z, \bar{z}, 0) + z + \bar{z})^3 \\
&= 3z^2\bar{z} + \cdots .
\end{aligned}$$

$$\begin{aligned}
u_t^3(-\tau) &= ((w(z, \bar{z}, -\tau) + ze^{-j\omega_0\tau} + \bar{z}e^{j\omega_0\tau})^3 \\
&= 3z^2\bar{z}e^{-j\omega_0\tau} + \cdots .
\end{aligned}$$

$$
\begin{aligned}
u_t(0)u_t(-\tau) &= (w(z,\bar{z},0)+z+\bar{z}) \\
&\quad \times (w(z,\bar{z},-\tau)+ze^{-j\omega_0\tau}+\bar{z}e^{j\omega_0\tau}) \\
&= z^2e^{-j\omega_0\tau}+z\bar{z}(e^{-j\omega_0\tau}+e^{j\omega_0\tau})+\bar{z}^2e^{j\omega_0\tau} \\
&\quad + z^2\bar{z}(w_{11}(0)e^{-j\omega_0\tau}+\frac{w_{20}(0)}{2}e^{j\omega_0\tau} \\
&\quad + w_{11}(-\tau)+\frac{w_{20}(-\tau)}{2})+\cdots .
\end{aligned}
$$

$$
\begin{aligned}
u_t^2(-\tau) &= ((w(z,\bar{z},-\tau)+ze^{-j\omega_0\tau}+\bar{z}e^{j\omega_0\tau})^2 \\
&= z^2e^{-2j\omega_0\tau}+\bar{z}^2e^{2j\omega_0\tau}+2z\bar{z} \\
&\quad +z^2\bar{z}(2e^{-j\omega_0\tau}w_{11}(-\tau)+e^{j\omega_0\tau}w_{20}(-\tau))+\cdots .
\end{aligned}
$$

$$
\begin{aligned}
u_t(0)u_t^2(-\tau) &= ((w(z,\bar{z},-\tau)+ze^{-j\omega_0\tau}+\bar{z}e^{j\omega_0\tau})^2 \\
&\quad \times (w(z,\bar{z},0)+z+\bar{z}) \\
&= z^2\bar{z}(e^{-2j\omega_0\tau}+2)+\cdots .
\end{aligned}
$$

Recall that

$$
\begin{aligned}
g(z,\bar{z}) &= \bar{q}^*(0).\mathcal{F}_0(z,\bar{z}) \\
&= g_{20}\frac{z^2}{2}+g_{11}z\bar{z}+g_{02}\frac{\bar{z}^2}{2}+g_{21}\frac{z^2\bar{z}}{2}+\cdots .
\end{aligned}
$$

After collecting the coefficients of $z^2, z\bar{z}, \bar{z}^2$ and $z^2\bar{z}$, we are in a position to calculate the coefficients of g_{20}, g_{11}, g_{02} and g_{21}, which we do as

$$
\begin{aligned}
g_{20} &= \bar{D}(2\xi_{xx}+2\xi_{xy}e^{-j\omega_0\tau}+2\xi_{yy}e^{-2j\omega_0\tau}) \\
g_{11} &= \bar{D}(2\xi_{xx}+2\xi_{xy}\cos\omega_0\tau+2\xi_{yy}) \\
g_{02} &= \bar{D}(2\xi_{xx}+2\xi_{xy}e^{j\omega_0\tau}+2\xi_{yy}e^{2j\omega_0\tau}) \\
g_{21} &= \bar{D}[2\xi_{xx}\{2w_{11}(0)+w_{20}(0)\} \\
&\quad +\xi_{xy}\{2w_{11}(0)e^{-j\omega_0\tau}+w_{20}(0)e^{j\omega_0\tau} \\
&\quad +2w_{11}(-\tau)+w_{20}(-\tau)\} \\
&\quad +\xi_{yy}\{4w_{11}(-\tau)e^{-j\omega_0\tau}+2w_{20}(-\tau)e^{j\omega_0\tau}\} \\
&\quad +6\xi_{xxx}+\xi_{xyy}\{2e^{-2j\omega_0\tau}+4\} \\
&\quad +\xi_{xxy}\{2e^{j\omega_0\tau}+4e^{-j\omega_0\tau}\}+6\xi_{yyy}e^{-j\omega_0\tau}].
\end{aligned}
$$

Note that from our earlier analysis (6.18), many of these terms vanish because of the coefficients.

Observe that in the expression for g_{21}, we have $w_{11}(0), w_{11}(-\tau), w_{11}(0)$ and $w_{11}(-\tau)$ which we still need to evaluate. Now for $\theta \in [-\tau, 0)$,

$$\begin{aligned} H(z,\bar{z},\theta) &= -2\Re\bar{q}^*(0).\mathcal{F}_0 q(\theta) \\ &= -2\Re g(z,\bar{z})q(\theta) \\ &= -g(z,\bar{z})q(\theta) - \bar{g}(z,\bar{z})\bar{q}(\theta) \\ &= -\left(g_{20}\frac{z^2}{2} + g_{11}z\bar{z} + g_{02}\frac{\bar{z}^2}{2} + \cdots\right) q(\theta) \\ &\quad -\left(\bar{g}_{20}\frac{\bar{z}^2}{2} + \bar{g}_{11}z\bar{z} + \bar{g}_{02}\frac{z^2}{2} + \cdots\right) \bar{q}(\theta) \end{aligned}$$

which, compared with (6.16), yields

$$H_{20}(\theta) = -g_{20}q(\theta) - \bar{g}_{02}\bar{q}(\theta) \tag{6.17}$$

$$H_{11}(\theta) = -g_{11}q(\theta) - \bar{g}_{11}\bar{q}(\theta). \tag{6.18}$$

We already noted that

$$(2j\omega_0 - A)w_{20}(\theta) = H_{20}(\theta) \tag{6.19}$$

$$-Aw_{11}(\theta) = H_{11}(\theta) \tag{6.20}$$

$$-(2j\omega_0 + A)w_{02}(\theta) = H_{02}(\theta). \tag{6.21}$$

From (6.14), (6.19) and (6.20), we get the following equations:

$$\begin{aligned} w'_{20}(\theta) &= 2j\omega_0 w_{20}(\theta) + g_{20}q(\theta) + \bar{g}_{02}\bar{q}(\theta) \\ w'_{11}(\theta) &= g_{11}q(\theta) + \bar{g}_{11}\bar{q}(\theta). \end{aligned}$$

Solving the above differential equations gives us

$$w_{20}(\theta) = -\frac{g_{20}}{j\omega_0}e^{j\omega_0\theta} - \frac{\bar{g_{02}}}{3j\omega_0}e^{-j\omega_0\theta} + Ee^{2j\omega_0\theta} \tag{6.22}$$

$$w_{11}(\theta) = \frac{g_{11}}{j\omega_0}e^{j\omega_0\theta} - \frac{\bar{g_{11}}}{j\omega_0}e^{-j\omega_0\theta} + F, \tag{6.23}$$

for some E, F, yet to be determined. Now for $H(z, \bar{z}, 0) = -2\Re\bar{q}^*.\mathcal{F}_0 q(0) + \mathcal{F}_0$,

$$\begin{aligned} H_{20}(0) &= -g_{20}q(0) - \bar{g}_{02}\bar{q}(0) \\ &\quad + \kappa(2\xi_{xx} + 2\xi_{xy}e^{-j\omega_0\tau} + 2\xi_{yy}e^{-2j\omega_0\tau}) \\ H_{11}(0) &= -g_{11}q(0) - \bar{g}_{11}\bar{q}(0) \\ &\quad + \kappa(2\xi_{xx} + 2\xi_{xy}\cos\omega_0\tau + 2\xi_{yy}). \end{aligned}$$

From (6.14), (6.19) and (6.20), we get

$$\begin{aligned} \kappa\xi_x w_{20}(0) + \kappa\xi_y w_{20}(-\tau) - 2j\omega_0 w_{20}(0) &= g_{20}q(0) + \bar{g}_{02}\bar{q}(0) \qquad (6.24) \\ &\quad +\kappa(2\xi_{xx} + 2\xi_{xy}e^{-j\omega_0\tau} + 2\xi_{yy}e^{-2j\omega_0\tau}) \\ \kappa\xi_x w_{11}(0) + \kappa\xi_y w_{11}(-\tau) &= g_{11}q(0) + \bar{g}_{11}\bar{q}(0) \qquad (6.25) \\ &\quad +\kappa(2\xi_{xx} + 2\xi_{xy}\cos\omega_0\tau + 2\xi_{yy}). \end{aligned}$$

We have the solution for $w_{20}(\theta)$ and $w_{11}(\theta)$ from (6.22) and (6.23) respectively. Hence, we evaluate $w_{11}(0), w_{11}(-\tau), w_{11}(0)$ and $w_{11}(-\tau)$, substitute into (6.24) and (6.25) respectively, and calculate E, F as

$$E = \frac{\phi_1}{\kappa\xi_x + \kappa\xi_y e^{-2j\omega_0\tau} - 2j\omega_0}$$

$$F = \frac{\phi_2}{\kappa\xi_x + \kappa\xi_y}, \qquad (6.26)$$

where

$$\begin{aligned} \phi_1 &= (\kappa\xi_x - 2j\omega_0)\left(\frac{g_{20}}{j\omega_0} + \frac{\bar{g_{02}}}{3j\omega_0}\right) \\ &\quad + \kappa\xi_y\left(\frac{g_{20}}{j\omega_0}e^{-j\omega_0\tau} + \frac{\bar{g_{02}}}{3j\omega_0}e^{j\omega_0\tau}\right) \\ &\quad + \text{RHS of (6.24)} \end{aligned}$$

$$\begin{aligned} \phi_2 &= -\xi_x\left(\frac{g_{11}}{j\omega_0} - \frac{\bar{g_{11}}}{j\omega_0}\right) \\ &\quad - \xi_y\left(\frac{g_{11}}{j\omega_0}e^{-j\omega_0\tau} - \frac{\bar{g_{11}}}{j\omega_0}e^{j\omega_0\tau}\right) \\ &\quad + \text{RHS of (6.25).} \end{aligned}$$

All the quantities required for the computation associated with the stability analysis of the Hopf bifurcation have been completed. The analysis can be performed using (5):

$$\begin{aligned}
c_1(0) &= \frac{j}{2\omega_0}\left(g_{20}g_{11} - 2|g_{11}|^2 - \frac{1}{3}|g_{02}|^2\right) + \frac{g_{21}}{2} \\
\mu_2 &= \frac{-\Re c_1(0)}{\rho'(0)} \\
P &= \frac{2\pi}{\omega_0}(1 + T_2\epsilon^2 + O(\epsilon^4)) \\
T_2 &= -\left(\frac{\Im c_1(0) + \mu_2\omega'(0)}{\omega_0}\right) \\
\beta_2 &= 2\Re c_1(0) \\
\epsilon &= \sqrt{\frac{\mu}{\mu_2}},
\end{aligned}$$

where $c_1(0)$ is called the Lyapunov coefficient. The conditions that help us verify the stability of the Hopf bifurcation are as follows:

1. The sign of μ_2 determines the type of bifurcation. If $\mu_2 > 0$ then it is a supercritical Hopf; $\mu_2 < 0$ means it is subcritical.
2. The sign of β_2, the Floquet exponent, determines the stability of the bifurcating periodic solutions. The periodic solutions are asymptotically orbitally stable if $\beta_2 < 0$ and unstable if $\beta_2 > 0$. If $\rho'(0) > 0$ then supercriticality of the bifurcating solution also establishes asymptotic orbital stability.
3. For small $|\mu|$, the period of the bifurcating solutions given by (6.27) reduces to $(2\pi/\omega_0)$ as $|\mu| \to 0$.
4. The bifurcating periodic solutions have the asymptotic form

   $$u(t, \mu(\epsilon)) = 2\epsilon\Re[e^{j\omega_0 t}] + \epsilon^2\Re[Ee^{2j\omega_0 t} + F] + O(\epsilon^3),$$

   for $0 \leq t \leq P(\epsilon)$. Thus we can determine the stability and periodicity of the bifurcating solutions with the above results as each system parameter transitions into instability.

Nature of Hopf bifurcation and stability of limit cycles

Using the numerical model (2.2) of pupillary reflex, we generate values of the parameters α, γ, τ to satisfy the Hopf condition (3.5) for a particular pupil area A^*:

$$\alpha\tau\sqrt{\left(\frac{\gamma}{\alpha\beta A^*}\right)^2 - 1} = \cos^{-1}\left(\frac{\alpha\beta A^*}{\gamma}\right).$$

The critical values of parameters used are:

$$\alpha_c = 2.3/\sec, \tau_c = 0.1358 \text{ sec}, \gamma_c = -10/\sec$$

for $A^* = 16\text{mm}^2$ and $\beta = g'(A^*) = 0.048\text{mm}^{-2}$, which remain constant. Each of these parameters are now perturbed from their critical values K_c to $K_c + \mu$, where μ is the bifurcation parameter. Limit cycles are generated as parameters transition into values that drive the system to instability. Bifurcation diagrams plot the steady state maxima and minima of these limit cycles as a function of the respective bifurcation parameters.

Pupillary constant α: Clearly, the bifurcation parameter is negative, since the system is driven to instability as α decreases from its critical value. We find that for any choice of $\mu \in (-0.1\alpha_c, 0.1\alpha_c)$, $\mu_2 < 0$. The resulting Hopf is, thus, *subcritical*. Also, the corresponding Floquet exponent β_2 is negative, so the bifurcating periodic solution is *asymptotically orbitally stable*.

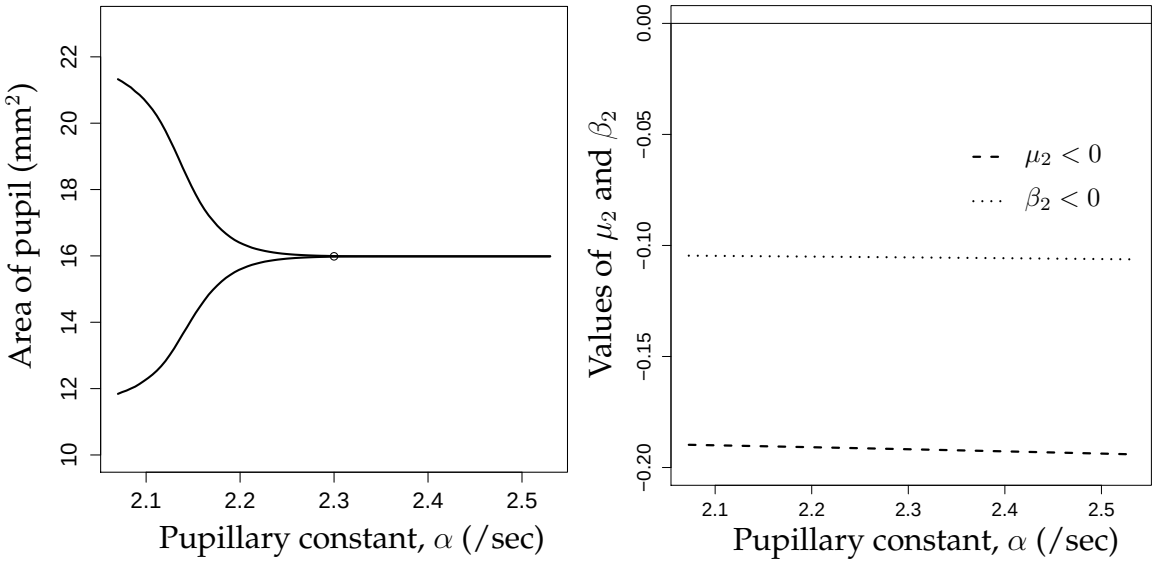

Figure 6.2: Bifurcation diagram generated with variation in pupillary constant α. The Hopf is found to be subcritical, and limit cycles stable. $A^* = 16mm^2$, $\gamma = -10/\sec$, $\tau = 0.1358\sec$.

Neural delay τ: Increasing the time delay drives the system into instability. We find that for any choice of $\mu \in (-0.1\tau_c, 0.1\tau_c)$, $\mu_2 > 0$. The resulting Hopf is, thus, *supercritical*. The Floquet exponent β_2 is negative, so the bifurcating periodic solution is *asymptotically orbitally stable*.

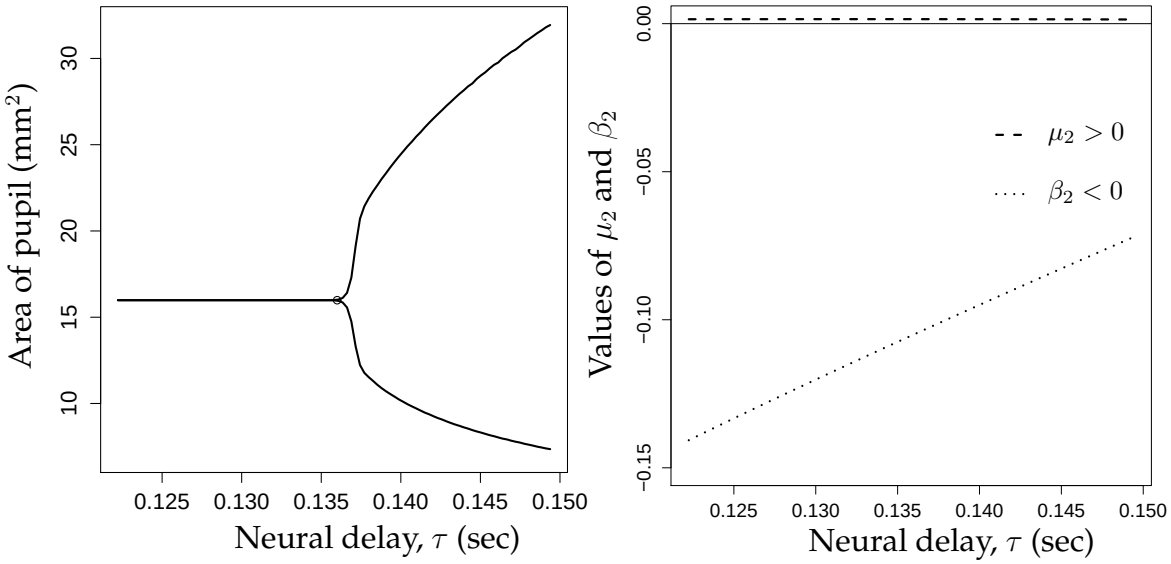

Figure 6.3: Bifurcation diagram generated with variation in neural delay τ. The Hopf is found to be supercritical, and limit cycles stable. $A^* = 16mm^2$, $\alpha = 2.3/\sec$, $\gamma = -10/\sec$.

Neural constant γ: Increasing the magnitude of γ drives the system into instability. We find that for any choice of $\mu \in (-0.1\gamma_c, 0.1\gamma_c)$, $\mu_2 < 0$, so the resulting Hopf is *subcritical*. The Floquet exponent β_2 is negative, so the bifurcating periodic solution is *asymptotically orbitally stable*.

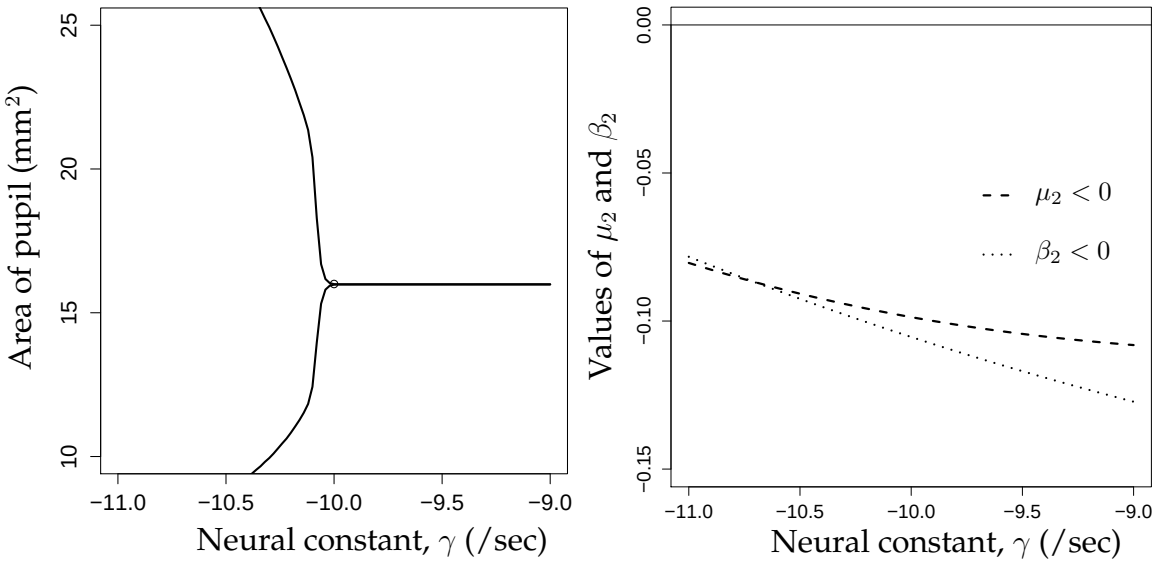

Figure 6.4: Bifurcation diagram generated with variation in neural constant γ. The Hopf is found to be subcritical, and limit cycles stable. $A^* = 16mm^2$, $\alpha = 2.3/\text{ sec}$, $\tau = 0.1358$ sec.

The table below summarises the results of our bifurcation analysis.

Parameter	*Nature of Hopf bifurcation*	*Stability of bifurcating solution*
Pupillary constant, α	Subcritical	Asymptotically Orbitally Stable
Neural delay, τ	Supercritical	Asymptotically Orbitally Stable
Neural constant, γ	Subcritical	Asymptotically Orbitally Stable

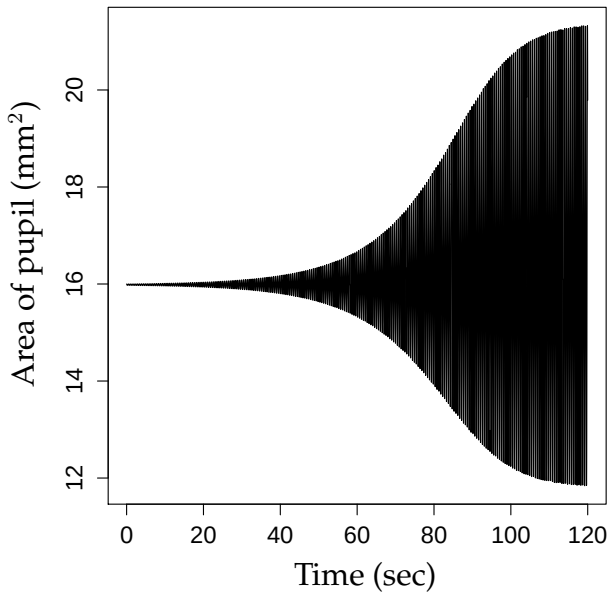

Figure 6.5: Limit cycles generated when pupillary constant α exceeds its critical value, driving the system to instability.

Design considerations

A subcritical Hopf bifurcation is undesirable in any dynamical system. We find that variations in the pupillary constant and neural constant may drive the system to instability through a subcritical Hopf. Thus, the pupillary response is difficult to regulate once a loss of local stability occurs.

But the takeaway from nature is that parameter values can be chosen well within the stable region, while still ensuring a desired level of performance in terms of rate of convergence and robustness.

CHAPTER 7

Conclusions

Pupillary light reflex finds extensive study in the literature as a physiological system. However, analysis from the perspective of design remains largely unexplored. This would take into account key performance metrics like stability, rate of convergence and robustness. The basis of our work is the non-linear, time delayed model of pupillary reflex proposed in (6). Our results offer guidelines to choose system parameters so as to maintain local stability and achieve a desired level of performance.

We linearised the pupillary reflex model and proposed a transfer function to model outputs to small perturbations in intensity of light. The neural delay was found to be an intrinsic parameter, and not part of the feedback. Some local stability properties of the model were analysed. This included a sufficient condition that assures stability regardless of the value of delay. We plotted stability charts that revealed trade-offs between the neural delay and other parameter values so as to keep the system stable. Our investigation into the rate of convergence produced a necessary and sufficient condition to keep the pupillary response overdamped. In fact, parameter values can be tuned to achieve a desired level of damping. The robustness of the model was measured for uncertainties in parameter values, offering insight to choose parameters appropriately. We proved that variations in all parameter values can induce a loss of local stability via Hopf bifurcations. Large neural constants were found to give rise to limit cycles through a subcritical Hopf, which is undesirable, in which case the pupillary response is difficult to control once a loss of stability occurs.

Avenues for further research

Notions of reachability and observability for the pupillary reflex model are yet to be characterised. All the biological aspects of the model have not been taken into consideration. For instance, the dynamic response of the retinal and

neural components of the pupillar reflex have been modelled just by a single delay term. These can be coupled through another set of differential equations, and a similar analysis can be repeated to give more accurate results.

REFERENCES

[1] K. J. ASTROM AND R. M. MURRAY, *Feedback Systems: An Introduction for Scientists and Engineers*. Princeton University Press, 2010.

[2] G. A. BOCHAROV AND F. A. RIHAN, *Numerical Modelling in Biosciences using Delay Differential Equations*, Journal of Computational and Applied Mathematics, 125 (2000), pp. 183-199.

[3] P. C. BRESSLOFF AND C. V. WOOD, *Spontaneous Oscillations in a Nonlinear Delayed-feedback Shunting Model of the Pupil Light Reflex*, Physics Review E, 58 (1998), pp. 3597–3605.

[4] P. C. BRESSLOFF, C. V. WOOD AND P. A. HOWARTH, *Nonlinear Shunting Model of the Pupil Light Reflex*, Proceedings: Biological Sciences, 263 (1996), pp. 953-960.

[5] B. D. HASSARD, N. D. KARAZINOFF AND Y. H. WAN, *Theory and Applications of Hopf Bifurcation*. Cambridge, U.K: Cambridge Univ. Press, 1981.

[6] A. LONGTIN AND A. G. MILTON, *Insight into the Transfer Function, Gain, and Oscillation Onset for the Pupil Light Reflex Using Nonlinear Delay-Differential Equations*, Biological Cybernetics, 61 (1989), pp. 51-58.

[7] V. F. PAMPLONA, M. M. OLIVEIRA AND G. V. G. BARANOSKI, *Photorealistic Models for Pupil Light Reflex and Iridal Pattern Deformation*, ACM Trans. Graph, 28 (2009), pp. 1-12.

[8] G. RAINA, *Local Bifurcation Analysis of Some Dual Congestion Control Algorithms*, IEEE Transactions on Automatic Control, 50 (2005), pp. 1135–1146.

[9] L. STARK, *Stability, Oscillations, and Noise in the Human Pupil Servomechanism*, Proceedings of the IRE, 47 (1959), pp. 1925 - 1939.

[10] C. TILMANT, L. SARRY, G. GINDRE AND J. Y. BOIRE, *Monitoring and Modeling of Pupillary Dynamics*, Engineering in Medicine and Biology Society,

2003. Proceedings of the 25th Annual International Conference of the IEEE, 1 (2003), pp. 678-681.

[11] H. U. VOSS, *A Backward Time Shift Filter for Nonlinear Delayed-feedback Systems*, Physics Letters A, 279 (2001), pp. 207-214.